Title

Uranyl Tris(benzoate) Photocatalysts for Site-Selective Hydrocarbon Functionalization

Journal

Journal of the American Chemical Society, 148(21)

ISSN

0002-7863

Authors

Herrera, Gabriel

Wong, Anthony

Fiszbein, David

et al.

Publication Date

2026-06-03

DOI

10.1021/jacs.6c01402

Uranyl tris(benzoate) photocatalysts for site selective hydrocarbon functionalization

Gabriel Herrera, Anthony Wong, David Fiszbein, Betsy A. Haibel, Jaden Lara, Nicholas J. Katzer, John F. Hartwig*, Polly L. Arnold*

University of California, Berkeley, and Lawrence Berkeley National Laboratory; Berkeley, California CA 94720, US.

*Corresponding author. Email: pla@berkeley.edu

KEYWORDS uranyl; carboxylate; O-ligand; C-H activation; photocatalysis

ABSTRACT: The uranyl dication ($[UO_2]^{2+}$) is a highly active photocatalyst for the functionalization of inert C_{sp3}–H bonds by direct hydrogen atom abstraction (HAA). However, photocatalysis by the uranyl ion remains underexplored. Most reports are limited to reactions catalyzed by simple uranyl salts, such as uranyl nitrate $[UO_2(NO_3)_2{\bullet}6H_2O]$ (**U^{NO3}**). We report a set of uranyl tris(benzoate) complexes **1-R** containing strongly coordinating and tunable equatorial ligands that are inert to photodamage and control access to the oxo groups. These catalyst variants with appropriate aryl substituents undergo catalytic reactions at C–H bonds by HAA, and the selectivity and reactivity of this step depend on the ligand framework and is distinct from that of **U^{NO3}** or other photoactive oxo complexes, such as decatungstate, that lack ancillary ligands. Finally, consistent with the strong, stable axial U–O bond, reaction with exogenous radical acceptors outcompetes radical rebound, enabling C–C and C–N bond formation from the alkyl radical intermediate. Regioselective alkylation and functionalization of a broad range of substrates results, and this photocatalysis shows that modulation of equatorial ligands on $[UO_2]^{2+}$ can influence the reactivity and selectivity of photocatalytic C–H bond functionalization.

INTRODUCTION

Reactive, high-valent d-block metal-oxo groups are the active site in many enzymes and the reactive unit in many molecular catalysts that functionalize C–H bonds by processes involving hydrogen atom abstraction (HAA). Typically, these oxo complexes are generated as reactive intermediates, and the scope of the resulting C–H bond functionalization is limited by their propensity to undergo radical rebound processes, leading to hydroxylation, halogenation, or pseudohalogenation (Figure 1a). [1–8]

In special cases, stable d-block metal-oxo complexes can be rendered reactive by photoexcitation. For example, the high-valent tungsten oxo group in the thermally stable decatungstate cluster $[n\mathrm{Bu_4N}]_4[W_{10}O_{32}]$ catalyzes reactions by a HAA step that is triggered by UV light. Because the W–O bond is strong, it resists radical rebound processes and has been widely investigated as a photocatalyst for the functionalization of C–H bonds beyond oxidation.[9,10] However, derivatization of the decatungstate ion is more challenging than derivatization of the d-block metal-oxo catalyst precursors and has not been reported. Thus, the site selectivity of the HAA step is controlled by the inherent electronic properties of the $W_{10}O_{32}$ unit. Organocatalytic systems that mediate photocatalytic HAA are also known, but these typically require a co-photocatalyst for activation and provide only limited control over site selectivity.[11–16] In particular, aryl ketone catalysts have not been shown to enable site selective photocatalytic C–H functionalization[17–19], highlighting the opportunity for a stable, modular metal oxo-based catalyst that combines tunable selectivity with reactivity beyond radical rebound.

In contrast to these described d-block metal-oxo systems, the uranyl dication is monomeric and contains a stable metal-oxo unit. Absorption of ~400-460 nm visible light causes the ground-state uranyl ion to undergo a ligand-to-metal charge transfer (LMCT) to generate a highly oxidizing intermediate (approx. +2.6 V vs SHE) with radical character localized on the oxo ligands. The oxo unit of this excited state abstracts hydrogen atoms from unactivated alkyl C–H bonds (Figure 1b).[20–24]

Because the strong U–OH bond generated after HAA, the uranyl ion catalyzes the conversion of C(sp^3)–H bonds into C–F, C–C and C–O bonds by the generation of nucleophilic alkyl radicals that add to electrophilic radical acceptors (Figure 1b).[25–38] However, the uranyl ion remains underexplored as a photocatalyst, despite this high reactivity. Most reports are limited to reactions catalyzed by simple uranyl salts, such as uranyl nitrate hexahydrate ($UO_2(NO_3)_2{\bullet}6H_2O$), abbreviated here as **U^{NO3}**, in which the equatorial plane is weakly coordinated by labile nitrate and/or water molecules.[22] Because of the absence of ancillary ligands, the selectivity for reaction at one C–H bond vs another is governed by the intrinsic reactivity and electronic preferences of the uranyl excited state and the properties of the C–H bonds in the substrate, and the yields are defined by the reactivity of the unligated UO_2^{2+} unit and variations of reaction conditions like time, solvent, and irradiation intensity.

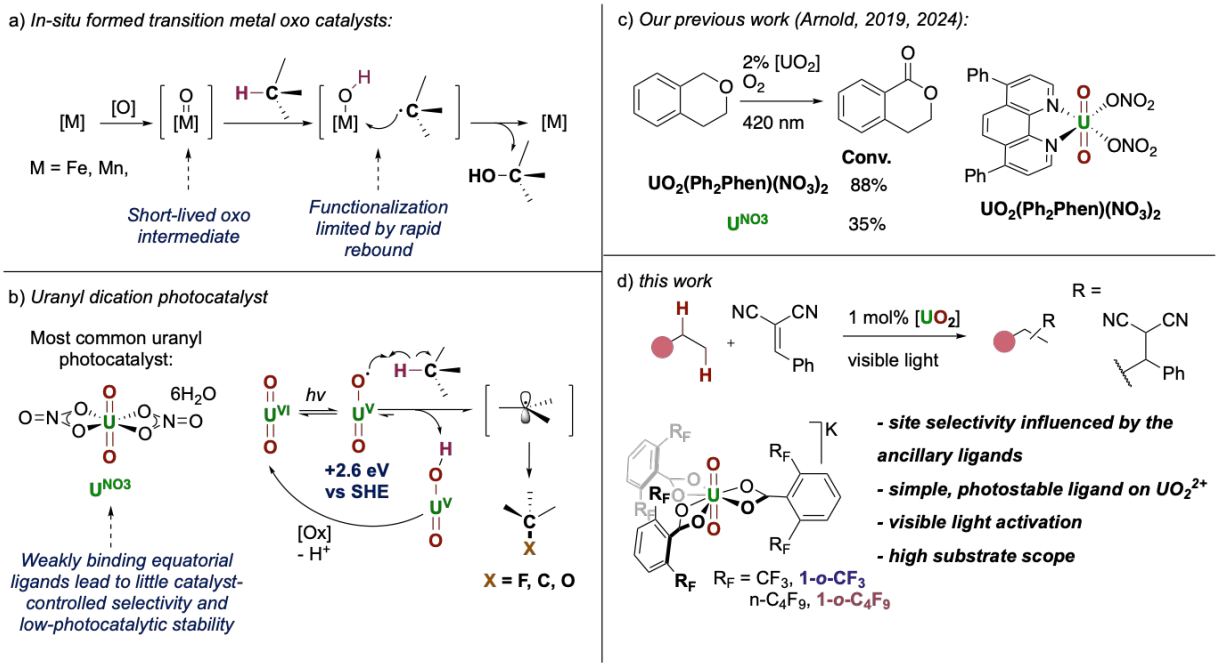

Figure 1. a) Hydrogen Atom Abstraction (HAA) from an alkane by a highly reactive d-block-oxo ion and subsequent radical rebound to form an alcohol; b) uranyl nitrate, $\mathbf{U^{NO3}}$ and the key steps proposed for its catalyzed C–H bond functionalization reactions; c) previous work on the use of ancillary ligands to increase reactivity of the uranyl ion; d) this work on uranyl tris(benzoate) complexes as highly reactive, modular photocatalysts for site selective HAA.

Unlike decatungstate, $[UO_2]^{2+}$ binds a range of ancillary ligands in the equatorial plane. If these ligands could remain coordinated under the reaction conditions, if they survived the strongly oxidizing reaction environment, and if the oxo reactivity were retained when the ligands are coordinated, this equatorial ligand set could modulate the activity, lifetime, and selectivity of the catalyst.

Few studies have been published on ligated uranyl complexes as photocatalysts. Most of the known examples involve heterogeneous, uranyl-organic frameworks (UOFs). Although these heterogeneous photocatalysts are more photostable and recyclable than UO_2^{2+}, modifications of the substituents in these frameworks to control selectivity have not been reported. One of us has shown previously that the photocatalysts $(Ph_2PhenUO_2)(X)_2$ (X = Cl, NO_3) functionalize benzylic C–H bonds with greater reactivity than $\mathbf{U^{NO3}}$ (Figure 1c), but the yields of functionalized products from reactions catalyzed by the parent $\mathbf{U^{NO3}}$ were higher than those catalyzed by $(Ph_2Phen)UO_2(X)_2$.[24,39] Other chelating ligands such as salen and acetylacetonate were used to support homogeneous uranyl photocatalysts but none has yet shown sufficient stabilization of the highly oxidizing uranyl excited state, resulting in decreased reactivity and no difference in site selectivity from that of $\mathbf{U^{NO3}}$.[40,41]

Here, we show that the coordination of benzoate ligands in the equatorial plane generates uranyl photocatalysts that are both longer lived and more reactive than $\mathbf{U^{NO3}}$. In addition, the steric and electronic properties of these benzoate ligands can be varied to modulate reactivity and selectivity, making the product distribution distinct from that of reactions catalyzed by $\mathbf{U^{NO3}}$ or other metal-oxo photocatalysts like decatungstate. Perfluoroalkyl substituents on the benzoate lead to a particularly reactive catalyst and steer reactivity toward more sterically accessible C–H bonds by modulation of the steric environment around the uranyl–oxo group (Figure 1d). This allows for HAA of a range of C–H bonds, including cycloalkanes (with BDEs of 96-99 kcal/mol) and even the primary C–H bonds of linear alkanes (with BDEs of 100 kcal/mol).

RESULTS

I. Synthesis of uranyl tris(benzoate) complexes

We began our effort to create discrete, ligated uranyl complexes that would react selectively with C–H bonds by preparing a variety of uranyl tris(benzoate) complexes containing substituents on the arene of varied steric and electronic properties (Figure 2a). We varied the substituents on the arenes to assess the effect of the electronic and steric properties of the ligand on the reactivity of these complexes toward catalytic reactions involving HAA. Complexes **1-R** were synthesized from $\mathbf{U^{NO3}}$ and 3.1 equivalents of the appropriate potassium benzoate salt in MeCN at room temperature (see SI).

^{1}H NMR spectra of **1-R** contained one set of aromatic proton resonances, suggesting a symmetric complex in solution. The UV-vis absorption spectra of acetonitrile solutions of **1-R** contain a series of vibronically coupled absorption bands centered at 431-433 nm, with only

small variations between benzoate complexes. The major absorption in each spectrum shows a vibronic progression of roughly 625 cm^{-1}, extending the absorption envelope over 410-470 nm. Furthermore, the molar absorption coefficient of all the **1-R** complexes is larger than that of $\mathbf{U^{NO3}}$, although the precise value depends on the benzoate substituents. Excitation at λ_{ex}=431 nm leads to fluorescence within an envelope centered around 500 nm that displays the anticipated vibronic progression of about 833 cm^{-1} (Figure S9-11) in the 450-600 nm range for complexes **1-*o*-CF$_3$**, **1-*m*-CF$_3$**, and **1-*p*-CF$_3$**.

The solid-state FTIR spectra all contain an absorption expected for the uranyl stretch at frequencies between 900-950 cm^{-1}. In solution, the value of ν_{asymm} increases in the order 907 cm^{-1} < 922 cm^{-1} < 937 cm^{-1} for **1-*p*-OMe**, **1-*o*-*t*Bu**, and **1-*p*-CF$_3$**, as would be anticipated for three complexes in which the ligand is progressively less electron donating. The solution spectra of **1-*o*-*t*Bu** contain a single absorption at 919 cm^{-1}, but the solid-state spectra contain two at 914 cm^{-1} and 924 cm^{-1}, which we attribute to geometries arising from the coordination of the potassium countercation to O atoms from both carboxylate and an oxo which is observed in the solid-state structure, see below.

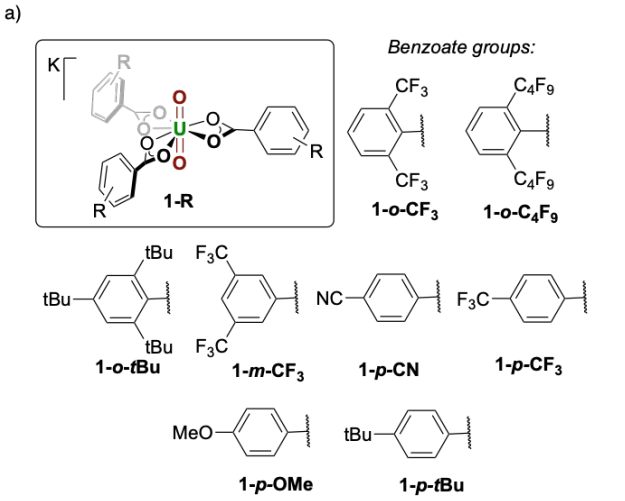

Figure 2. a) Eight uranyl tris(benzoate) complexes **1-R**; b) Visible-light electronic absorption spectra of complexes **1-R** and $\mathbf{U^{NO3}}$.

Consistent with this, the IR spectra of complexes with no crystallographically-observed K-coordination are the same in solution and in the solid state. The diffusion coefficients of **1-*o*-CF$_3$**, **1-*o*-C$_4$F$_9$**, and **1-*p*-OMe** from DOSY NMR spectroscopy are nearly identical, indicating that they are likely monomeric and of similar in size in solution, see Figures SI24-26.

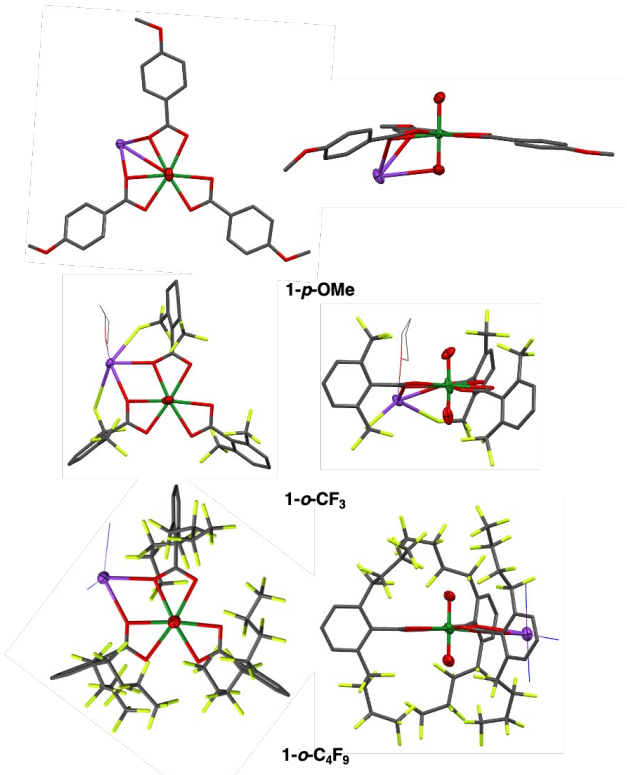

Figure 3. Molecular structures of **1-*p*-OMe**, **1-*o*-CF$_3$** and **1-*o*-C$_4$F$_9$**; top view on the left and side-on view on the right. Where shown, probability ellipsoids are set at 50%, peripheral groups are shown wireframe. Lattice solvent and H atoms are omitted for clarity. Green = U; red = O; grey = C; yellow = F; magenta = K; blue = N.

The solid-state structures of all the **1-R** complexes contain three benzoate ligands coordinated in the equatorial plane of the uranium atom, forming an eight-coordinate, anionic 'ate' uranyl complex with six coordinated oxygen atoms in the equatorial plane (Figure 3). When present, the *ortho*-substituents (**1-*o*-CF$_3$**, **1-*o*-C$_4$F$_9$,** and **1-*o*-*t*Bu**) on the aryl carboxylates force the aryl groups to lie normal to the equatorial plane, thereby creating a pocket in which the uranyl oxo ligands are sterically protected. The solid-state structures of **1-*o*-CF$_3$**, **1-*o*-C$_4$F$_9$**, and **1-*p*-OMe** also contain a potassium counter cation that sits between two benzoate carboxylates, with bonds to one O atom of two carboxylate ligands, but this binding mode of the potassium does not significantly perturb the U–O bond

distance. The solid-state structure of **1-*p*-OMe**, for instance, features three crystallographically distinct uranyl ions in the asymmetric unit, all with various interactions between potassium counter cations and either a uranyl oxo or a uranyl-coordinated carboxylate oxygen. The distances of the U-O_{COAr} bonds with the oxygens associated to a K^+ ion in three distinct uranyl units range from 2.410(4)-2.514(4) Å, whereas the distances of the U-O_{COAr} bonds without potassium range from 2.410(4)-2.443(3) Å. In addition, the presence or type of additional potassium-carboxylate interaction does not significantly impact the uranyl U=O bond lengths. The U=O bond distances in all of the crystallographically distinct uranyl units reported here are within 1.770(4)-1.785(5) Å. The solid-state structures of **1-*o*-*t*Bu** and **1-*p*-CN** also contain a single potassium counter cation between two benzoate carboxylates, but the potassium in both complexes also interacts with one of the two uranyl oxo groups.

II. Photocatalyzed C–H functionalization

Table 1: Uranyl photocatalyzed alkylation of cyclohexane

Reaction conditions: 500 µmol 2a (5 equiv), 100 µmol **3a** (1

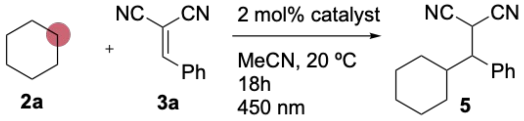

2a **3a** **5**

Entry	Catalyst	Deviation	% yield 5
1	**U^{NO3}**	none	36%
2	**1-*o*-CF3**	none	**>99%**
3	**1-*o*-CF3**	1 mol% cat.	**>99%, 90%**
4	**1-*o*-CF3**	0.5 mol% cat, 36h	**>99%**
5	**1-*o*-C_4F_9**	none	80%
6	**1-*p*-CF_3**	none	36%
7	**1-*p*-CN**	none	36%
8	**1-*m*-CF_3**	none	23%
9	**1-*o*-*t*Bu**	none	20%
10	**1-*p*-OMe**	none	12%
11	**1-*p*-*t*Bu**	none	trace
12	**U^{NO3}**	1 mol% cat., acetone as solvent	24%
13	**1-*o*-CF3**	no light	0%
14	**NA**	no photocatalyst	0%

equiv), 2 mol% photocatalyst, 1 mL anhydrous MeCN, N_2 atmosphere, 450 nm, 20 °C, 18 h; Yields determined by ^{1}H NMR spectroscopy with MeOAc as internal standard.

We evaluated the activity of complexes **1-R** as photocatalysts for the functionalization of C–H bonds by examining the C–H alkylation of cyclohexane (**2a**) with 2-benzylidenemalononitrile (**3a**) as the radical acceptor. We anticipated that these reactions would follow the mechanism outlined in Error: Reference source not foundb involving initial HAA by the U=O excited state (II. Photocatalyzed C–H functionalization). Each catalyst was tested with a 2 mol% loading, and uranyl nitrate (**U^{NO3}**) was also tested to serve as a benchmark.

Among the series of complexes **1-R**, complex **1-*o*-CF_3** was the most active photocatalyst, delivering >99% yield of the alkylated product, versus just 36% yield with **U^{NO3}** (II. Photocatalyzed C–H functionalization, entries 1 and 2). The high efficiency of **1-*o*-CF_3** was retained, even at lower catalyst loadings, with >99% conversion of the alkene observed at both 1 mol% and 0.5 mol% loading after 24 h and 36 h of irradiation, respectively (entries 3 and 4). The reaction catalyzed by **1-*o*-C_4F_9** delivered the same product in 62% yield (II. Photocatalyzed C–H functionalization, entry 5). The activities of the other catalysts, such as **1-*p*-CF_3**, **1-CN**, and **1-*m*-CF_3**, were comparable to that of **U^{NO3}** (36% yield, entries 6 and 7) or slightly lower (entry 8). The activity of complexes with more electron-donating ligands, such as **1-*o*-*t*Bu** and **1-*p*-OMe**, was lower (20% and 12% conversion, entries 9 and 10) than the other photocatalysts, including **U^{NO3}**, while **1-*p*-*t*Bu** was entirely inactive (entry 11). Control reactions in the absence of light or catalyst formed no product (entries 13 and 14). The Ravelli group previously reported a high yield for this transformation with 8 mol% **U^{NO3}** and acetone as solvent. From reactions conducted with 1 mol% loading of **U^{NO3}** in acetone in their SI they report only 26% yield of **5**, very similar to our measurement of 24% conversion with 1 mol% loading of **U^{NO3}** in acetone in our reaction setup (Table 1, entry 12).

We then determined and compared the initial rates of the reactions with 2 mol% **1-*o*-CF_3**, **1-*m*-CF_3**, **1-*p*-CF_3**, **1-*p*-OMe**, and **U^{NO3}**. The rates for cyclohexane alkylation were 20.3 mM/h, 4.33 mM/h, 4.60 mM/h, 0.769 mM/h, and 9.99 mM/h, respectively (Figure 4). Continued irradiation of **1-*m*-CF_3** and **1-*p*-CF_3** led to 90% and 82% yields of **5** after 72 h, respectively. These data imply that the higher product yields after 18 h irradiation between the benzoate catalysts are due to a faster rate of product formation for **1-*o*-CF_3**. Thus, the incorporation of three 2,6-bis(trifluoromethyl)benzoate ligands around the uranyl center dramatically enhances photocatalytic reactivity of the uranyl ion for the functionalization of inert C–H bonds. The reactivity of **1-*o*-CF_3** is higher than that of the other catalysts in the series, but we have been unable to correlate catalyst activity with a particular measured parameter. We are currently seeking to understand the electronic features that lead to higher reactivity of a given uranyl photocatalyst.

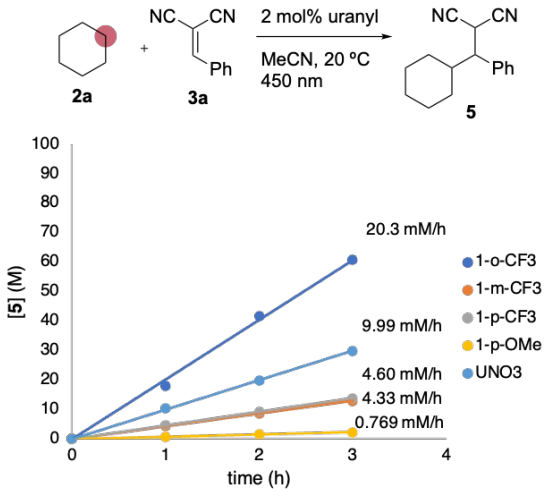

Figure 4: Initial rates of formation of **5** from reactions catalyzed by a series of uranyl complexes; the concentrations of **5** were determined by GC-FID with n-dodecane as internal standard

To compare the reactivity and selectivity of our new photocatalyst and $\mathbf{U^{NO3}}$, we evaluated the scope of substrates that react with **1-*o*-CF$_3$** or $\mathbf{U^{NO3}}$ under otherwise identical conditions, Error: Reference source not found. The scope of substrates that react with catalyst **1-*o*-CF$_3$** is greater than that with $\mathbf{U^{NO3}}$, and the high reactivity of **1-*o*-CF$_3$** under those conditions enabled this evaluation of the substrate scope to be investigated with 1 mol% catalyst loading. For substrates that react with both catalysts, the reactions catalyzed by **1-*o*-CF$_3$** generally occurred in higher yields. For example, reactions of cyclic alkanes (**4–7**) formed the alkylated products in 86-99% yield when catalyzed by **1-*o*-CF$_3$**, but in just 8–33% yield when catalyzed by $\mathbf{U^{NO3}}$. Reactions of substrates with benzylic groups (**8–11**) were especially sensitive to the catalyst identity; reactions catalyzed by **1-*o*-CF$_3$** afforded 33-99% yields of the functionalized product, whereas the reactions catalyzed by $\mathbf{U^{NO3}}$ occurred to <1% yield and <1% conversion of the alkene in all cases. Based on literature precedent, we assume this difference in activity of the catalysts with these substrates results from the unproductive quenching of the excited state by aromatic units that can more readily access the uranyl oxo group in $\mathbf{U^{NO3}}$ than in **1-*o*-CF$_3$**.[42] The yields of reactions catalyzed by **1-*o*-CF$_3$** were also consistently higher than those catalyzed by $\mathbf{U^{NO3}}$ on polycyclic substrates (**12**, **13**) (e.g. 54-67% catalyzed by **1-*o*-CF$_3$** versus 7-13% catalyzed by $\mathbf{U^{NO3}}$).

The higher activity of **1-*o*-CF$_3$** than of $\mathbf{U^{NO3}}$ extends to aldehydes (**15, 16**) and cyclic ethers (**18**, **19**). These substrates undergo functionalization catalyzed by **1-*o*-CF$_3$** in yields ranging from 71-99%, while the reactions with $\mathbf{U^{NO3}}$ occur in much lower yield (6-25%). The only exception is dimethyl acetamide (**17**), which reacts in similar yields when catalyzed by $\mathbf{U^{NO3}}$ as when catalyzed by **1-*o*-CF$_3$**. Complex substrates also reacted. For example, (–)-ambroxide (**20**) underwent alkylation at the secondary carbon alpha to oxygen in high yield (84%) when catalyzed by **1-*o*-CF$_3$** but in just 8% yield when catalyzed by $\mathbf{U^{NO3}}$. Collectively, these results highlight the greater reactivity and versatility of **1-*o*-CF$_3$** for the functionalization of C–H bonds than of $\mathbf{U^{NO3}}$.

The reactions of cyclohexane (**2a**) and cyclooctane (**2d**) with a series of radical acceptors catalyzed by **1-*o*-CF$_3$** are shown at the bottom of Table 2. The reactions with alkenes containing varying aromatic groups to form products **21-23** occurred in quantitative to near-quantitative yields. The reaction of the alkene substituted with a cycloalkyl group generated addition product **24** in 72% yield. The reaction with di-*tert*-butylazidodicarboxylate (DBAD, **25**) catalyzed by **1-*o*-CF$_3$** formed product containing a C–N bond in 32% yield.

Table 2: Scope of C–H functionalization catalyzed by 1-*o*-CF$_3$ and U^{NO3}

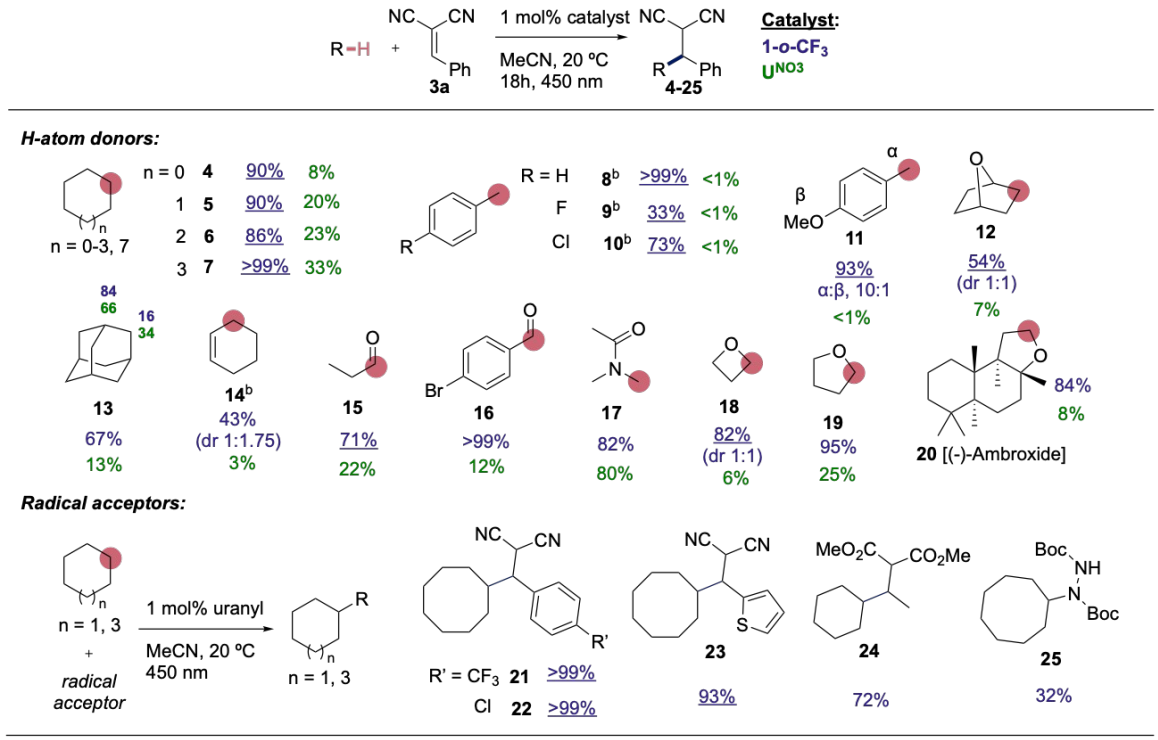

[a] Reaction conditions: 500 µmol R–H (5 equiv), 100 µmol **3a** (1 equiv), 1 mol% photocatalyst, 1 mL anhydrous MeCN, N_2 atmosphere, 450 nm, 20 ºC, 18h; [b] Irradiation for 36h; [c] Only three equivalents C–H substrate used; underlined = isolated yields, otherwise ^{1}H NMR spectroscopic yields with MeOAc internal standard.

III. Site selectivity for C–H functionalization

As discussed in the introduction, these photocatalysts were designed to influence the site selectivity of the functionalization of C(sp^3)–H bonds. Indeed, the site selectivity of the reactions of *n*-hexane (**26**) as a model substrate and 2-benzylidenemalononitrile (**2b**) as the radical acceptor with **1-*o*-CF$_3$** and **1-*o*-C$_4$F$_9$** as catalyst is distinct from that of **U^{NO3}.** Catalyst **1-*o*-CF$_3$** and, particularly, **1-*o*-C$_4$F$_9$** reacts with higher selectivity for the more sterically accessible C–H bonds than does **U^{NO3}** (Error: Reference source not found). Tetra-n-butylammonium decatungstate (**TBADT**) was also used as a photocatalyst, though the irradiation wavelength was reduced to 390 nm. The distribution of products from alkylation at the C1, C2, and C3 positions varies from 0:44:56, respectively, with **U^{NO3}** to 5:54:41 with **1-*o*-CF$_3$** to 17:56:27 with **1-*o*-C$_4$F$_9$** and 8:59:33 with **TBADT**. The site selectivity of the alkylation of **26** with **1-*o*-CF$_3$** is similar to that with **TBADT** under these conditions. In contrast, the more sterically hindered **1-*o*-C$_4$F$_9$** favors alkylation at the sterically accessible C1 and C2 positions of **26**. This result emphasizes that the ligands on the uranyl photocatalysts influence the site selectivity for C–H functionalization. This type of catalyst-control has not been demonstrated with prior metal-oxo HAA photocatalysts such as **TBADT**. The yield of the reaction is highest with **1-*o*-CF$_3$** (97%), followed by **1-*o*-C$_4$F$_9$** (52%). The reaction with **U^{NO3}** gave only 18% yield, and **TBADT** gave trace product at 450 nm irradiation, but the yield increased to 36% at 390 nm. For all three of these complexes, the selectivity remains consistent throughout the reaction time, suggesting that the active catalyst is unchanged during the reaction (Figure SI34-36). Furthermore, all of the reported yields and selectivities were measured at the point when the yield of the product reached its maximum value. The selectivity of **1-*o*-*t*Bu** is similar to that of **1-*o*-C$_4$F$_9$**, but the product yield is significantly lower (4%).

A distinct selectivity of the fluoroalkyl-substituted uranyl benzoate catalysts for HAA was observed for reactions of all the substrates tested. The tendency for reaction of the more sterically hindered C–H bonds of linear and branched alkanes (**27**, **28**) was higher for reactions catalyzed by complex **1-*o*-C$_4$F$_9$** than for those catalyzed by **1-*o*-CF$_3$** or **U^{NO3}**. The yields were also higher when catalyzed by **1-*o*-CF$_3$** and **1-*o*-C$_4$F$_9$** than when catalyzed by **U^{NO3}**. For example, the reaction of cyclopentyl methyl ether (**29**) favors the primary C–H bond over the tertiary C–H bond (60:40), whereas the reaction catalyzed by **1-*o*-CF$_3$** (35:65) and **U^{NO3}** (15:85) favor reaction at the tertiary C–H bonds and the yield of the reaction is higher when catalyzed by **1-*o*-CF$_3$** and **1-*o*-C$_4$F$_9$** (>99% and 84%, respectively) than by **U^{NO3}**. Any products derived from a beta-scission mechanism were not included in the distribution of products from reaction of substrate **29** with olefin **3a** because the two alkylation products shown

were by far the major products, as determined by ^{1}H NMR and GC-MS analysis of the crude reaction mixture after 18 h of irradiation.

Likewise, the selectivity for reaction at the primary versus tertiary benzylic C–H bonds of *p*-cymene (**30**) are higher with **1-*o*-C$_4$F$_9$** (91:9) than with **1-*o*-CF$_3$** (75:25), and the reactions occurred in good to high, 53% and 83% yields with **1-*o*-C$_4$F$_9$** and **1-*o*-CF$_3$**. In contrast, the reaction with **U^{NO3}** gave the alkylated product in <1% yield, and the selectivity could not be measured for such small amounts of material. Similarly, the selectivity for the primary versus secondary C–H bonds of tetraethylsilane (**31**) with **1-*o*-C$_4$F$_9$** (96:4) was higher than that with **1-*o*-CF$_3$** (80:20), and the yields were 90%-99%. Again, the reaction catalyzed by **U^{NO3}** gave only trace product.

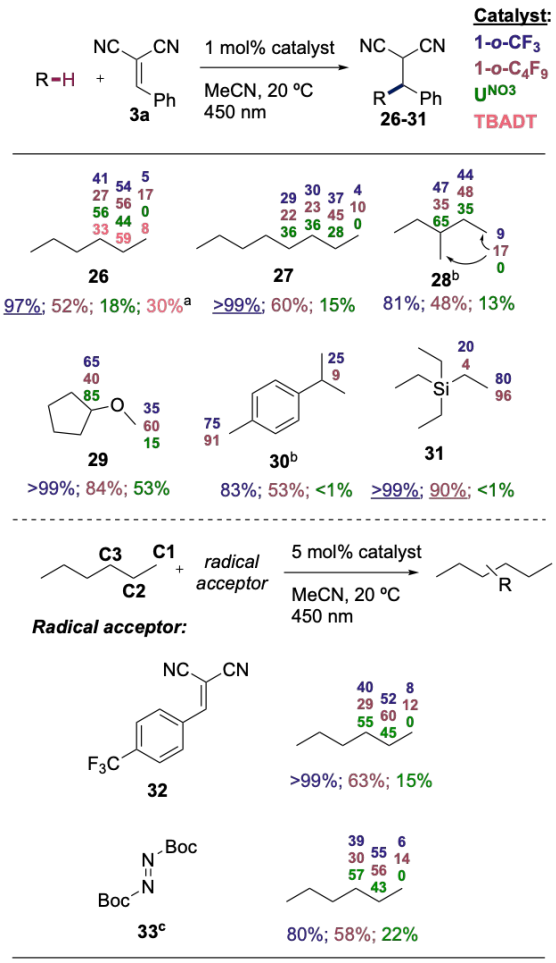

Reaction conditions: 500 µmol R–H (5 equiv), 100 µmol **3a** (1 equiv), 1 mol% photocatalyst, 1 mL anhydrous MeCN, N_2 atmosphere, 450 nm, 20 °C, 18 h; [a]390 nm LED was used; [b]Irradiation for 36 h; underlined = isolated yields, otherwise ^{1}H NMR spectroscopic yields with MeOAc internal standard.

Table 3: Site selective C–H alkylation with different uranyl photocatalysts

We next sought to determine if selectivity is maintained across different radical acceptors. If the selectivity is dictated by HAA and each of the radicals formed reacts fully with the radical acceptor, then the site selectivity should not be significantly affected by the identity of the acceptor. To test this prediction, we conducted the functionalization of n-hexane with a series of radical acceptors. As shown in Table 3, the site selectivity of reactions with another aryl-substituted alkene and even with the azo acceptor (**32** and **33**, respectively) were nearly identical to each other and to those with 2-benzylidienemalononitrile (**3a**). These results indicate that site selectivity is likely controlled exclusively by the HAA step.

IV. Catalyst lifetime

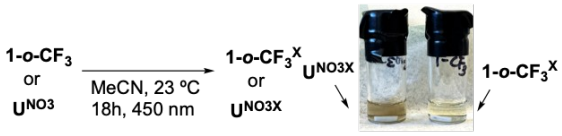

Scheme 1: Irradiation of uranyl complexes before addition of substrate. Reaction conditions: 1 µmol **1-*o*-CF$_3$** and **U^{NO3}**, 1 mL anhydrous MeCN, N_2 atmosphere, 450 nm, 20 °C, 18h.

To assess the effect of the ancillary ligand on the catalyst lifetime, we conducted a series of experiments to determine the fate of the complexes with and without the benzoate on $[UO_2]^{2+}$. In the absence of a stabilizing ligand environment, previous literature suggests that many uranyl(V) intermediates undergo spontaneous intermolecular disproportionation, forming uranyl(VI) and insoluble uranium(IV) oxides.[43–46] We hypothesized that the carboxylate ligands might suppress the dimerization of U(V) intermediates that leads to disproportionation and deactivation of the catalyst by precipitation of U(IV). To test this idea, we irradiated both **1-*o*-CF$_3$** and **U^{NO3}** with 450 nm light in the absence of alkane and alkene for 18 h. After irradiation, the catalyst solution containing **U^{NO3}** had turned a dark gray color, with visible precipitate present, but irradiation of **1-*o*-CF$_3$** led to little change in color of the solution and no precipitation (Scheme 1). The uranium species present in the vials after irradiation will be referred to as **U^{NO3X}** and **1-*o*-CF$_3^X$**, respectively. After addition of both alkane (**2a**) and alkene (**3a**) and irradiation for an additional 18 h, the reaction with **1-*o*-CF$_3^X$** delivered **5** in 86% yield while the reaction with **U^{NO3X}** gave only trace product (Table 4, entries 1 and 2).

Quantitative ^{19}F NMR spectroscopic analysis of the solutions of the reactions catalyzed by **1-*o*-CF$_3$**, **1-*o*-C$_4$F$_9$**, **1-*p*-CF$_3$**, and **1-*m*-CF$_3$** in Scheme 1b was conducted to determine the fate of the catalysts under the standard reaction conditions. In every case, the benzoate catalyst remained intact in near quantitative amounts (Table 4, >95%, entries 3-5), suggesting that the equatorial ligands are responsible for the high stability of these complexes. Furthermore, the high reactivity of **1-*o*-CF$_3$** and **1-*o*-C$_4$F$_9$** is likely due to more than just catalyst longevity because **1-*o*-CF$_3$** and **1-*o*-C$_4$F$_9$** lead to higher yields of the functionalized products than do **1-*p*-CF$_3$** or **1-*m*-CF$_3$**. **1-*o*-CF$_3$** was isolated from the reaction mixture after 18h of irradiation, with 58% recovery (Table 4, entry 6). This result further supports the high stability of **1-*o*-CF$_3$** under the reaction conditions.

Cyclic voltammetry (CV) of complexes **1-*o*-CF$_3$** and **1-*m*-CF$_3$** in MeCN was conducted to assess the difference in the U(VI)/U(V) reduction potentials of these two complexes and to determine if the difference in reactivity parallels the difference in reduction potential. The CVs of these complexes contain an irreversible reduction peak at -1.40 V and -1.69 V versus Fc/Fc$^+$, respectively; we attribute this to the U(VI) to U(V) reduction (Figures SI12 and SI13). The CV of **U^{NO3}** contains an irreversible reduction wave at the much higher potential of -0.464 V vs Fc/Fc$^+$ in MeCN (Figure SI14). Between the two benzoate catalysts, the higher reactivity of **1-*o*-CF$_3$** can be attributed to its lower reduction potential in the ground state and, presumably, the corresponding excited states. The low reactivity of **U^{NO3}** can be attributed to the observed catalyst decomposition during irradiation. Due to the irreversibility of the reduction of the uranyl tris(benzoate) complexes, an excited state potential could not be accurately calculated for these complexes.

Table 4: Cyclohexane alkylation under standard conditions with various uranyl photocatalysts showing stability of tris(benzoate) complexes

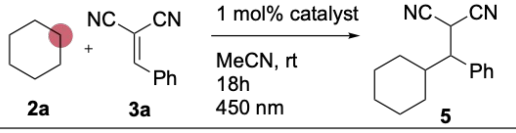

2a 3a 5

Entry	Catalyst	% remaining catalyst	% yield 5
1	1-*o*-CF$_3^X$	NA	86%
2	U^{NO3X}	NA	trace
3	1-*o*-CF$_3$	>95%	>99%
4	1-*o*-C$_4$F$_9$	>95%	49%
5	1-*m*-CF$_3$	>95%	10%
6	1-*o*-CF$_3$[a]	58%[b]	>99%

Yield determined by ^{1}H NMR spectroscopy with MeOAc as internal standard.; remaining catalyst determined by integration of the ^{19}F NMR signal against 1-fluoronaphthalene as internal standard. [a]2 mol% loading; [b]isolated yield after completion of the reaction.

V. Mechanistic studies

To gain information on the HAA step of this reaction, Stern-Volmer quenching analyses were conducted and kinetic isotope effects were measured for reactions catalyzed by a series of uranyl complexes. Stern-Volmer quenching experiments with 20 mM **1-R** in anhydrous MeCN solutions and cyclohexane as the excited state quencher revealed a Stern-Volmer constant (K_{SV}) of 14.6 M^{-1} for **1-*o*-CF$_3$** (SI29). This constant is higher than the corresponding values of 8.16 M^{-1} and 8.05 M^{-1} for **1-*p*-CF$_3$** and **1-*m*-CF$_3$**, (SI31-33). The larger value for **1-*o*-CF$_3$** implies that HAA by **1-*o*-CF$_3$** is faster than by the other benzoate photocatalysts.

We also measured the KIE of the reaction of cyclohexane from reactions run side by side. The KIE determined from measurements of the initial rates of

parallel reactions with **1-*o*-CF$_3$** as catalyst was 5.0 (Figure 5a), while that with **1-*o*-C$_4$F$_9$** as catalyst was 11.0. These KIE values suggest that HAA is the rate determining step in these reactions. Furthermore, the high KIE value with **1-*o*-C$_4$F$_9$** as catalyst suggests that the HAA step occurs with a contribution from tunneling.

The spectroscopic and kinetic data are consistent with the mechanism shown in Figure 5b. First, the ground state uranyl(VI) is excited to a triplet state that cleaves the C–H bond to form a carbon-centered radical and a uranyl(V) hydroxide complex. The carbon-centered radical then reacts with the alkene or related radical acceptor to yield an electron-poor radical. The catalyst, then, would be regenerated either by oxidation of the U(V) to U(VI) by the electron-poor radical, forming a stabilized carbanion, followed by proton transfer or by direct hydrogen atom transfer from the uranyl(V) hydroxide to the electron-poor radical. When a mono-substituted olefin, such as methyl acrylate, was employed as the radical acceptor, less than 1% product was observed. This observation is consistent with inefficient regeneration of the starting U(VI) complex because the α-radical intermediate does not react with the U(V) intermediate to regenerate the catalyst. The primary KIE rules out two potential alternative mechanisms, one in which HAA occurs by the olefin **3a** by energy transfer from the excited uranyl complex, and one in which addition of the radical is reversible. The first mechanism is ruled out because HAA by the olefin would lead to identical KIE values for reactions with different uranyl photocatalysts, but the KIE values (5.0 and 11.0) are distinct for reactions of **1-*o*-CF$_3$** and **1-*o*-C$_4$F$_9$**, respectively. The second mechanism can be ruled out because the large primary KIE indicates that HAA is irreversible. Therefore, any influence on product distribution would have to arise from rearrangement of the resulting carbon radical. Although reversible radical addition could increase the lifetime of this radical and enable rearrangement, changing the identity of the radical acceptor has little effect on the product distribution. Thus, reversibility is likely not influencing product distribution, ruling out this mechanism.

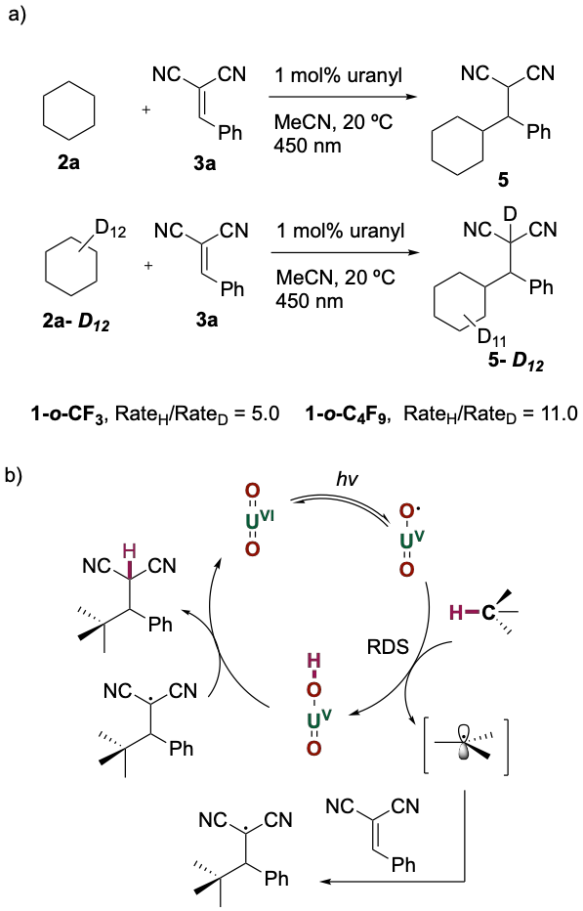

Figure 5: a) kinetic isotope effects of 1-*o*-CF$_3$ and 1-*o*-C$_4$F$_9$ using cyclohexane-H$_{12}$ and D$_{12}$; products were tracked by GC-FID with n-dodecane internal standard b) proposed mechanism for uranyl photocatalyzed C–H alkylation.

CONCLUSIONS

We have described a set of uranyl benzoate complexes that catalyze the functionalization of both unactivated and activated alkyl C–H bonds by hydrogen-atom abstraction under visible light irradiation and have shown how changing the ancillary ligand modulates the activity and site selectivity of the catalyst for functionalization of C–H bonds to form C–C and C–N bonds. This new class of uranyl-based photocatalysts, **1-R** possess several advantages over the benchmark **U^{NO3}** photocatalyst. First, the three equatorial benzoate ligands in **1-R** remain bound under catalytic conditions, thereby contributing to the combination of high stability, reactivity, and selectivity of these catalysts. The photocatalytic reactivity of the catalysts bearing electron-withdrawing and ortho-substituted groups is significantly enhanced over that of complexes bearing electron-donating groups or either meta- or para-electron-withdrawing groups, indicating the importance of ligand electronic and steric properties for the photoreactivity. Second, the visible-light absorption coefficient of the **1-R** complexes is greater than that of **U^{NO3}** while maintaining similar

excitation energies, thereby enabling more efficient photochemical activation with visible light. Third, ortho substituents create a defined pocket around the reactive oxo group, leading to substrate-catalyst interactions that enable ligand-controlled site selectivity for the HAA step. Finally, the **1-R** catalysts are protected from interactions with unsaturated substrates that form exciplexes and lead to unproductive energy transfer that deactivates $\mathbf{U^{NO3}}$. By mitigating this interaction, the scope of the substrates for the catalytic functionalization is broadened. Together, these features confer higher reactivity and broader substrate scope and offer a platform for modulating selectivity by ligand design. We anticipate that this catalyst framework will expand reactivity further with diverse radical acceptors and greater control over C–H functionalization.

ASSOCIATED CONTENT

Supporting Information

The Supporting Information is available free of charge on the ACS Publications website.

CCDC numbers for X-ray data (2485065-2485069) and additional crystallographic details, experimental procedures, spectroscopic and spectrometric data for reactions, compounds, and catalyses (PDF).

AUTHOR INFORMATION

Corresponding Authors

pla@berkeley.edu, jhartwig@berkeley.edu

ACKNOWLEDGMENT

The catalysis studies were supported by the Catalysis Program (FWP CH030201) and some structural studies (AW) were carried out in the Heavy Element Program (FWP CH030203), all in the U.S. Department of Energy (DOE), Office of Science, Office of Basic Energy Sciences, Chemical Sciences, Geosciences, and Biosciences Division, at the Lawrence Berkeley National Laboratory. The Catalysis Laboratory in the DOE Catalysis Program also provided resource and instrumentation used in this work and some diffraction data were collected at Beamline 12.2.1 of the Advanced Light Source, which is a DOE Office of Science User Facility. All of these DOE programs and facilities operate under contract no. DE-AC02-05CH11231. Raman spectra were acquired using instrumentation provided by the Liquid Sunlight Alliance, which is supported by the US Department of Energy, Office of Science, Office of Basic Energy Sciences, Fuels from Sunlight Hub under award no. DE-SC0021266. We thank Drs. Hasan Celik, Raynald Giovine, and Pines Magnetic Resonance Center's Core NMR Facility (PMRC Core) for spectroscopic assistance. The instruments used in this work are supported by the National Science Foundation under Grant No. 2018784 and the National Institutes of Health (NIH) under grant no 1S10RR016634-01. We also thank the NIH for support for G.H. (fellowship under FAIN 5F31GM149158). This project has also received funding for some of the early synthetic work from the European Research Council (ERC) under the European Union's Horizon 2020 research and innovation programme (grant agreement No 740311).

REFERENCES

(1) Chen, M. S.; White, M. C. Combined Effects on Selectivity in Fe-Catalyzed Methylene Oxidation. *Science* **2010**, *327* (5965), 566–571. https://doi.org/10.1126/science.1183602.

(2) Nanjo, T.; de Lucca, E. C. Jr.; White, M. C. Remote, Late-Stage Oxidation of Aliphatic C–H Bonds in Amide-Containing Molecules. *J. Am. Chem. Soc.* **2017**, *139* (41), 14586–14591. https://doi.org/10.1021/jacs.7b07665.

(3) Ahn, C.; Gomez, A.; Hartmann, M. A.; White, M. C. Selective Methylene Oxidation in α,β-Unsaturated Carbonyl Natural Products. *Nature* **2025**. https://doi.org/10.1038/s41586-025-09742-0.

(4) White, M. C.; Zhao, J. Aliphatic C–H Oxidations for Late-Stage Functionalization. *J. Am. Chem. Soc.* **2018**, *140* (43), 13988–14009. https://doi.org/10.1021/jacs.8b05195.

(5) Lyakin, O. Y.; Talsi, E. P.; Bryliakov, K. P. Bioinspired Oxidations of C–H Groups Mediated by Nonheme Complexes of Late Transition Metals Co, Ni, and Cu. *ACS Catal.* **2025**, *15* (20), 17525–17547. https://doi.org/10.1021/acscatal.5c05705.

(6) Wang, V. C.-C.; Maji, S.; Chen, P. P.-Y.; Lee, H. K.; Yu, S. S.-F.; Chan, S. I. Alkane Oxidation: Methane Monooxygenases, Related Enzymes, and Their Biomimetics. *Chem. Rev.* **2017**, *117* (13), 8574–8621. https://doi.org/10.1021/acs.chemrev.6b00624.

(7) Gunay, A.; Theopold, K. H. C–H Bond Activations by Metal Oxo Compounds. *Chem. Rev.* **2010**, *110* (2), 1060–1081. https://doi.org/10.1021/cr900269x.

(8) Borovik, A. S. Role of Metal–Oxo Complexes in the Cleavage of C–H Bonds. *Chem. Soc. Rev.* **2011**, *40* (4), 1870–1874. https://doi.org/10.1039/C0CS00165A.

(9) Ravelli, D.; Fagnoni, M.; Fukuyama, T.; Nishikawa, T.; Ryu, I. Site-Selective C–H Functionalization by Decatungstate Anion Photocatalysis: Synergistic Control by Polar and Steric Effects Expands the Reaction Scope. *ACS Catal.* **2018**, *8* (1), 701–713. https://doi.org/10.1021/acscatal.7b03354.

(10) Singh, P. P.; Sinha, S.; Gahtori, P.; Tivari, S.; Srivastava, V. Recent Advances of Decatungstate Photocatalyst in HAT Process. *Org. Biomol. Chem.* **2024**, *22* (13), 2523–2538. https://doi.org/10.1039/D4OB00213J.

(11) Mahmudov, K. T.; Pombeiro, A. J. L. Control of Selectivity in Homogeneous Catalysis through Noncovalent Interactions. *Chem. – Eur. J.* **2023**, *29* (26), e202203861. https://doi.org/10.1002/chem.202203861.

(12) Zhou, R.; Liu, H.; Tao, H.; Yu, X.; Wu, J. Metal-Free Direct Alkylation of Unfunctionalized Allylic/Benzylic Sp3 C–H Bonds via Photoredox Induced Radical Cation Deprotonation. *Chem. Sci.* **2017**, *8* (6), 4654–4659. https://doi.org/10.1039/C7SC00953D.

(13) Fan, X.-Z.; Rong, J.-W.; Wu, H.-L.; Zhou, Q.; Deng, H.-P.; Tan, J. D.; Xue, C.-W.; Wu, L.-Z.; Tao, H.-R.; Wu, J. Eosin Y as a Direct Hydrogen-Atom Transfer Photocatalyst for the Functionalization of C–H Bonds. *Angew. Chem. Int. Ed.* **2018**, *57* (28), 8514–8518. https://doi.org/10.1002/anie.201803220.

(14) Ma, Z.-Y.; Li, M.; Guo, L.-N.; Liu, L.; Wang, D.; Duan, X.-H. Sulfonamide as Photoinduced Hydrogen-Atom Transfer Catalyst for Regioselective Alkylation of C(Sp3)–H Bonds Adjacent to Heteroatoms. *Org. Lett.* **2021**, *23* (2), 474–479. https://doi.org/10.1021/acs.orglett.0c03992.

(15) Yakubov, S.; Stockerl, W. J.; Tian, X.; Shahin, A.; Mandigma, M. J. P.; Gschwind, R. M.; Barham, J. P. Benzoates as Photosensitization Catalysts and Auxiliaries in Efficient, Practical, Light-Powered Direct C(Sp3)–H Fluorinations. *Chem. Sci.* **2022**, *13* (47), 14041–14051. https://doi.org/10.1039/D2SC05735B.

(16) Entgelmeier, L.-M.; Mori, S.; Sendo, S.; Yamaguchi, R.; Suzuki, R.; Yanai, T.; García Mancheño, O.; Ohmatsu, K.; Ooi, T. Zwitterionic Acridinium Amidate: A Nitrogen-Centered Radical Catalyst for Photoinduced Direct Hydrogen Atom Transfer. *Angew. Chem. Int. Ed.* **2024**, *63* (43), e202404890. https://doi.org/10.1002/anie.202404890.

(17) Breslow, R.; Rajagopalan, R.; Schwarz, J. Selective Functionalization of Doubly Coordinated Flexible Chains. *J. Am. Chem. Soc.* **1981**, *103* (10), 2905–2907. https://doi.org/10.1021/ja00400a088.

(18) Breslow, R.; Baldwin, S. W. Conversion of Cholestanol to 12-Oxocholestanol and to Cholest-14-Enol and-8(14)-Enol by Remote Oxidation. *J. Am. Chem. Soc.* **1970**, *92* (3), 732–734. https://doi.org/10.1021/ja00706a068.

(19) Capaldo, L.; Ravelli, D.; Fagnoni, M. Direct Photocatalyzed Hydrogen Atom Transfer (HAT) for Aliphatic C–H Bonds Elaboration. *Chem. Rev.* **2022**, *122* (2), 1875–1924. https://doi.org/10.1021/acs.chemrev.1c00263.

(20) Cowie, B. E.; Purkis, J. M.; Austin, J.; Love, J. B.; Arnold, P. L. Thermal and Photochemical Reduction and Functionalization Chemistry of the Uranyl Dication, [UVIO2]2+. *Chem. Rev.* **2019**, *119* (18), 10595–10637. https://doi.org/10.1021/acs.chemrev.9b00048.

(21) Hu, D. J., Xuefeng. Perspectives for Uranyl Photoredox Catalysis. *Synlett* **2021**, *32* (13), 1330–1342. https://doi.org/10.1055/a-1493-3564.

(22) Gao, P.; Shen, Z.; Chen, Y.; Jiang, T.; Ji, Z.; Zhao, G.; Yue, J.; Hu, Y.; Wang, X.; Huang, X.; Muhler, M.; Yin, L. A Review on Uranyl-Based Photocatalysts in Photocatalytic Organic Transformation. *J. Catal.* **2025**, *442*, 115900. https://doi.org/10.1016/j.jcat.2024.115900.

(23) Arnold, P. L.; Puig-Urrea, L.; Wells, J. A. L.; Yuan, D.; Cruickshank, F. L.; Young, R. D. Applications of Boroxide Ligands in Supporting Small Molecule Activation by U(Iii) and U(Iv) Complexes. *Dalton Trans.* **2019**, *48* (15), 4894–4905. https://doi.org/10.1039/C8DT05051A.

(24) Arnold, P. L.; Purkis, J. M.; Rutkauskaite, R.; Kovacs, D.; Love, J. B.; Austin, J. Controlled Photocatalytic Hydrocarbon Oxidation by Uranyl Complexes. *ChemCatChem* **2019**, *11* (16), 3786–3790. https://doi.org/10.1002/cctc.201900037.

(25) Wu, L.; Cao, X.; Chen, X.; Fang, W.; Dolg, M. Visible-Light Photocatalysis of C_{sp3}-H Fluorination by the Uranyl Ion: Mechanistic Insights. *Angew. Chem. Int. Ed.* **2018**, *57* (36), 11812–11816. https://doi.org/10.1002/anie.201806554.

(26) Mashita, T.; Tsushima, S.; Takao, K. Photocatalytic Oxygenation of Cyclohexene Initiated by Excitation of $[UO_2(OPCyPh_2)_4]^{2+}$ under Visible Light. *ACS Omega* **2019**, *4* (4), 7194–7199. https://doi.org/10.1021/acsomega.9b00635.

(27) He, W.-M.; Lin, Y.-W.; Yu, D.-H. Uranyl Photocatalysis: Precisely Controlled Oxidation of Sulfides with Ground-State Oxygen. *Sci ChinaChem* **2020**, No. 3, 291–293.

(28) Yu, J.; Zhao, C.; Zhou, R.; Gao, W.; Wang, S.; Liu, K.; Chen, S.; Hu, K.; Mei, L.; Yuan, L.; Chai, Z.; Hu, H.; Shi, W. Visible-Light-Enabled C–H Functionalization by a Direct Hydrogen Atom Transfer Uranyl Photocatalyst. *Chem Eur J* **2020**, *26* (69), 16521–16529. https://doi.org/10.1002/chem.202003431.

(29) Feng, Z. C(Sp3)-H Alkenylation Promoted by Uranyl Cation as a Visible-Light Photocatalyst. *J. Phys. Conf. Ser.* **2021**, *2079* (1), 012020. https://doi.org/10.1088/1742-6596/2079/1/012020.

(30) Zhou, Y.; Hu, D.; Li, D.; Jiang, X. Uranyl-Photocatalyzed Hydrolysis of Diaryl Ethers at Ambient Environment for the Directional Degradation of 4-O-5 Lignin. *JACS Au* **2021**, *1* (8), 1141–1146. https://doi.org/10.1021/jacsau.1c00168.

(31) Hu, D.; Zhou, Y.; Jiang, X. From Aniline to Phenol: Carbon-Nitrogen Bond Activation via Uranyl Photoredox Catalysis. *Natl. Sci. Rev.* **2022**, *9* (6). https://doi.org/10.1093/nsr/nwab156.

(32) Lv, S.; Li, Q.; Sang, J.-W.; Zhang, Y.; Wang, J.; Zhang, W.-D. Uranyl Nitrate as a Recyclable Homogeneous Photocatalyst for Selective Cross-Coupling of N-Substituted Amines and Indoles. *RSC Adv.* **2023**, *13* (18), 11929–11937. https://doi.org/10.1039/D3RA01037F.

(33) Zhang, S.-Y.; Tang, S.-B.; Jiang, Y.-X.; Zhu, R.-Y.; Wang, Z.-X.; Long, B.; Su, J. Mechanism of the Visible-Light-Promoted C(Sp3)–H Oxidation via Uranyl Photocatalysis. *Inorg. Chem.* **2024**, *63* (5), 2418–2430. https://doi.org/10.1021/acs.inorgchem.3c03347.

(34) Jiang, Y.-X.; Tang, S.-B.; Luo, Y.-Y.; Wang, Z.-X.; Li, Z.-K.; Su, J. Photocatalytic Cleavage of Unactivated C(Sp3)–H Bonds via the Uranyl Cation: Enabling the Allylation of Alkanes. *Org. Chem. Front.* **2025**. https://doi.org/10.1039/D5QO00649J.

(35) Hu, D.; Jiang, X. Stepwise Benzylic Oxygenation via Uranyl-Photocatalysis. *Green Chem.* **2022**, *24* (1), 124–129. https://doi.org/10.1039/D1GC04042A.

(36) Mao, Y.; Liu, Y.; Yu, L.; Ni, S.; Wang, Y.; Pan, Y. Uranyl-Catalysed C–H Alkynylation and Olefination. *Org. Chem. Front.* **2021**, *8* (21), 5968–5974. https://doi.org/10.1039/D1QO00932J.

(37) West, J. G.; Bedell, T. A.; Sorensen, E. J. The Uranyl Cation as a Visible-Light Photocatalyst for C(Sp3)–H Fluorination. *Angew. Chem. Int. Ed.* **2016**, *55* (31), 8923–8927. https://doi.org/10.1002/anie.201603149.

(38) Capaldo, L.; Merli, D.; Fagnoni, M.; Ravelli, D. Visible Light Uranyl Photocatalysis: Direct C–H to C–C Bond Conversion. *ACS Catal.* **2019**, *9* (4), 3054–3058. https://doi.org/10.1021/acscatal.9b00287.

(39) Rutkauskaite, R.; Zhang, X.; Woodward, A. W.; Liu, Y.; Herrera, G.; Purkis, J.; Woodall, S. D.; Sarsfield, M.; Schreckenbach, G.; Natrajan, L. S.; Arnold, P. L. The Effect of Ancillary Ligands on Hydrocarbon C–H Bond Functionalization by Uranyl Photocatalysts. *Chem. Sci.* **2024**, *15* (18), 6965–6978. https://doi.org/10.1039/D4SC01310G.

(40) Azam, M.; Al-Resayes, S. I.; Trzesowska-Kruszynska, A.; Kruszynski, R.; Kumar, P.; Jain, S. L. Seven-Coordinated Chiral Uranyl(VI) Salen Complex as Effective Catalyst for C–H Bond Activation of Dialkylanilines under Visible Light.

Polyhedron **2017**, *124*, 177–183. https://doi.org/10.1016/j.poly.2016.12.033.

(41) Clark, C. B.; Burnett, N. L.; Ruhren, A. N.; Talbott, E. D.; Eyubova, E.; Besson, C.; Panetier, J. A.; Swierk, J. R. Analyzing the Photophysics and Photochemistry of [UO2(Acetylacetonate)2(L)] Complexes. *Dalton Trans.* **2025**, *54* (33), 12667–12677. https://doi.org/10.1039/D5DT00668F.

(42) Mao, Y.; Bakac, A. Photocatalytic Oxidation of Toluene to Benzaldehyde by Molecular Oxygen. *J. Phys. Chem.* **1996**, *100* (10), 4219–4223. https://doi.org/10.1021/jp9529376.

(43) Arnold, P. L.; Pécharman, A.-F.; Love, J. B. Oxo Group Protonation and Silylation of Pentavalent Uranyl Pacman Complexes. *Angew. Chem. Int. Ed.* **2011**, *50* (40), 9456–9458. https://doi.org/10.1002/anie.201104359.

(44) Arnold, P. L.; Patel, D.; Wilson, C.; Love, J. B. Reduction and Selective Oxo Group Silylation of the Uranyl Dication. *Nature* **2008**, *451* (7176), 315–317. https://doi.org/10.1038/nature06467.

(45) Zegke, M.; Zhang, X.; Pidchenko, I.; Hlina, J. A.; Lord, R. M.; Purkis, J.; Nichol, G. S.; Magnani, N.; Schreckenbach, G.; Vitova, T.; Love, J. B.; Arnold, P. L. Differential Uranyl(v) Oxo-Group Bonding between the Uranium and Metal Cations from Groups 1, 2, 4, and 12; a High Energy Resolution X-Ray Absorption, Computational, and Synthetic Study. *Chem. Sci.* **2019**, *10* (42), 9740–9751. https://doi.org/10.1039/C8SC05717F.

(46) Ekstrom, A. Kinetics and Mechanism of the Disproportionation of Uranium(V). *Inorg. Chem.* **1974**, *13* (9), 2237–2241. https://doi.org/10.1021/ic50139a035.